IOP Publishing Measurement Science and Technology
Meas. Sci. Technol. **31** (2020) 065105 (10pp) https://doi.org/10.1088/1361-6501/ab7317

Parameterization-switching GNSS attitude determination considering the success rate of ambiguity resolution

Siyu Zhang[1,2], Guobin Chang[1,2], Chao Chen[1,2], Guoliang Chen[1,2] and Laihong Zhang[1,2]

[1] Key Laboratory of Land Environment and Disaster Monitoring, MNR, China University of Mining and Technology, Xuzhou 221116, People's Republic of China
[2] School of Environmental Science and Spatial Informatics, China University of Mining and Technology, Xuzhou 221116, People's Republic of China

E-mail: guobinchang@hotmail.com

Received 18 October 2019, revised 30 January 2020
Accepted for publication 5 February 2020
Published 3 April 2020

Abstract

The two key elements of GNSS attitude determination are the correct integer ambiguity resolution (IAR) and the choice of appropriate method. The least-squares ambiguity decorrelation adjustment method is normally used to fix ambiguities using float estimates. However, it is difficult to get all ambiguities fixed in real time. Therefore, a method of partial ambiguity resolution which considers the success rate of IAR and makes full use of the ambiguity information at each epoch is proposed. The ambiguities after decorrelation can be divided into fixed ambiguities and unfixed ambiguities considering the fixing success rate. At the next epoch, the fixed ones are treated as constants, while the float estimates of the unfixed ones, along with the corresponding covariance matrix, are treated as prior information or pseudo-measurements. The parameters of the attitude determination problem can be baseline coordinates (BCs) or attitude angles (AAs). BC parameterization, without considering the baseline constraints, has the merit of resulting in a linear model; however, it involves parameter redundancy, which reduces the model strength. AA parameterization, although avoiding parameter redundancy, brings in nonlinearity and hence linearization errors in the least-squares solution. The linearization errors decrease as the number of fixed ambiguities increases. A switching-parameterization method is proposed; namely, at any epoch, as long as there are at least three fixed double-difference ambiguities, AA parameterization is adopted, otherwise BC is adopted. Even with AA, BC is firstly estimated and then transformed to attitude estimates at which the nonlinear measurement equations are linearized and solved. To verify the performance of the proposed method, a comparative study is implemented with BC and AA methods in the static experiment. The results show that the proposed method can fix ambiguity faster and have better stability and accuracy. In addition, the yaw angle is consistent with the actual running route of the vehicle in the kinematic experiment.

Keywords: GNSS, attitude determination, parameterization switching, success rate, PAR

(Some figures may appear in colour only in the online journal)

1. Introduction

Attitude determination using GNSS has received broad attention in recent years. With its unique advantages, such as high precision, lack of drift, low cost and low power consumption [1, 2], it is widely used in aviation, aircraft, navigation, land and other fields [3–8]. The essence of GNSS attitude determination is placing an array of antennas onto a vehicle whose attitude information is to be determined by processing the data received by the antennas. A crucial challenge in this process, in

addition to the attitude calculation, is the resolution of carrier phase ambiguities [9]. Therefore, the research status will be introduced from two aspects, namely the integer ambiguity resolution (IAR) and attitude determination.

The methods of solving integer ambiguity include the ambiguity function method [10], the least-squares search method [11], the fast ambiguity solution method [12] and the least-squares ambiguity decorrelation adjustment (LAMBDA) method. Among all methods, the LAMBDA method is widely recognized as the most rigorous in theory and the most efficient to search for the optimal solution [13, 14]. Quite a few scholars have contributed to the IAR in GNSS attitude measurement [15, 16]. Due to the feature of unchanged baseline length in GNSS attitude determination, a constrained LAMBDA (C-LAMBDA) method is proposed, which is a non-trivial modification of the standard LAMBDA method [17]. Using C-LAMBDA, a high ambiguity resolution success rate and high computational efficiency will be achieved. It is suited to data processing in complicated kinematic environments [18]. The performance of the C-LAMBDA method is analyzed by means of extensive experimental testing including land, ship and aircraft experiments in literature [14]. However, for IAR, not all integer ambiguities can be easily fixed due to the randomness or the fact that the stochastic variability of the integer ambiguity estimator is too large to be neglected [19]. In general, only parts of ambiguities can be reliably fixed. The method of partial ambiguity resolution (PAR) is widely used in single-epoch IAR [20]. IAR is not necessarily implemented in a single-epoch manner, though this represents the most challenging case. Batch processing is not permitted in real-time applications, e.g. for GNSS attitude determination, the topic of this study. However, historical information corresponding to (unfixed) ambiguities can still be used at an epoch, through recursive methods, e.g. Kalman filtering or recursive least-squares, the latter being employed in this study. The existing PAR approaches are compared and analyzed in the framework of the recursive least-squares method. A subset of the ambiguity is selected to be fixed considering the fixing success rate, ratio values and other thresholds, and experimental results have shown that PAR can result in improvements in terms of both accuracy and quality control [21].

Attitude determination methods can be generally divided into two categories. One is accomplished in the position domain and the other is carried out in the measurement domain [22–24]. In the position domain, attitude will be obtained by transforming from the baseline vectors in the local level system (LLS) to the known baseline vectors in the body frame (BF); the former is calculated according to the baseline information in the WGS-84 coordinate system obtained directly from GNSS relative positioning processing. On the contrary, the attitude can be directly calculated from the linearized equation in the measurement domain. There may be parameter redundancy in the former even when the baseline constraints are taken into consideration. For instance, with p baselines, there are $2p$ parameters with the position-domain method, while the parameter number is always three with the measurement-domain method, as long as non-redundant attitude parameterizations are adopted, such as Euler angles, rotation vector and Rodrigues parameters [25, 26]. For $p \geq 2$, redundancy is introduced with the position-domain method. Parameter redundancy will decrease the model strength and increase the solution variance. If the baseline constraints are not considered, which is possible due to the merit of resulting in linearity of the model, the redundancy problem is more serious. Though avoiding parameter redundancy, the measurement-domain methods have their own demerit, namely the nonlinearity of the model. In the least-squares method, linearization is necessary which will inevitably introduce linearization errors. Clearly, the magnitude of the linearization errors directly depends on the accuracy of the initial attitude estimate at which the linearization is done. This initial attitude estimate is obtained from the transformation of the baseline solution. As long as there are at least three unambiguous carrier phase measurements, the baseline solution and hence the initial attitude estimate can be regarded sufficiently accurate. Then the linearization errors can be regarded as sufficiently small to be neglected. For brevity, in this work, the position-domain and measurement-domain methods are called the baseline coordinate (BC) and attitude angle (AA) approaches, respectively.

In this contribution, the PAR method is used in the recursive least-squares framework to resolve the integer ambiguities for the attitude determination. The integer ambiguities after decorrelation are divided into the fixed ambiguity group and the unfixed ambiguity group, considering the fixing success rate. The fixed ones are treated as constants. In addition, the float estimates of the unfixed ambiguities, along with the corresponding covariance matrix, will be retained to the next epoch, and be regarded as a set of pseudo-measurements to assist the IAR at that epoch. For both, the important precondition is that the corresponding satellite is still tracked without cycle slips or with cycle slips correctly repaired. Otherwise, for the former, namely the fixed ones, the double-difference (DD) measurement equation is used to calculate the float ambiguities by the least-squares method and LAMBDA is implemented. If the ambiguities cannot be fixed, it will be regarded as a part of the float estimates. For the latter, the prior information is obtained by the same way, although LAMBDA is not implemented. This is beneficial due to the improved overall accuracy and better quality control. For attitude determination, to avoid the demerits of the two parameterizations and combine their merits, a switching strategy is proposed. This strategy is simple and intuitive as follows. At any epoch, if there are at least three un-ambiguous carrier phase measurements, AA parameterization is employed, otherwise we employ BC. Considering that even in AA, BC is also firstly used to obtain the initial values to do the linearization, choosing the parameterization is essentially determining whether to do the linearization and hence the AA estimation. Note that three un-ambiguous carrier phase measurements make the three-parameter attitude determination problem properly determined, without considering low-accuracy pseudo-range measurements. Of course, the number of un-ambiguous carrier phase measurements larger than three would be a feasible alternative, without any essential

difference in the algorithm from that with three measurements. If the AA parameterization is not to be adopted, the unfixed ambiguity estimate in the initial BC solution is retained to the next epoch. Note that even with the BC parameterization, AA estimates can still be calculated, if necessary, although they are not used to linearize the nonlinear measurement equations.

The remainder of the paper is organized as follows: the second section introduces the parameterization-switching attitude determination method with PAR, which includes the PAR considering the bootstrapped success rate, BC and AA approaches. The third section demonstrates the performance of the proposed method through static and kinematic experiments. The fourth section presents the conclusions.

2. Parameterization-switching attitude determination method based on PAR

Either the BC or AA approach can be used for GNSS attitude determination. No matter which approach is used, the integer ambiguities must be solved correctly. In this contribution, the float ambiguities are calculated considering the correlation of integer ambiguities between epochs using recursive least-squares. PAR is used to fix the integer ambiguities with higher accuracy and better quality control. Furthermore, a parameterization switching strategy is employed for attitude determination in order to avoid the demerits of the two parameterizations and to combine their merits.

2.1. PAR considering the bootstrapped success rate

The fixing success rate is one of the critical reference criteria for whether the integer ambiguity can be correctly fixed, and it corresponds to the accuracy of the float ambiguity [19]. However, because of the complexity of the integer least-squares (ILS) ambiguity pull-in region and computational load of the integration of the multivariate probability density function, numerous researchers have taken the success rate computed with the integer bootstrapping method as the actual ILS success rate [27], which is also the case in this paper. The bootstrapped success rate is calculated by equation (1). In order to ensure that the ambiguities are correctly fixed, the ratio method is used to test the fixed ambiguities:

$$P_s = \prod_{i=1}^{m} \left(2\Phi \left(\frac{1}{2\sigma_{i|I}} \right) - 1 \right) \tag{1}$$

with

$$\Phi(x) = \frac{1}{\sqrt{2\pi}} \int_{-\infty}^{x} e^{-t^2/2} dt \tag{2}$$

where $\sigma_{i|I}$ are the diagonal elements of the covariance matrix of the converted ambiguity vector after LAMBDA processing.

Using the double-difference float ambiguities $\hat{\boldsymbol{n}}$, along with the corresponding covariance matrix, which can be easily computed in least-squares adjustment of the measurements, either with the BC or AA method detailed in the following, the following linear transformation is performed according to LAMBDA theory:

$$\hat{\boldsymbol{a}} = \boldsymbol{Z}^T \hat{\boldsymbol{n}}. \tag{3}$$

The bootstrapped success rate for each element of the vector in equation (3) is calculated by equation (1). The success rate is compared with a given threshold $\boldsymbol{P}_0$. According to this comparison, the float ambiguities after decorrelation are divided into two groups, as shown in equation (4), and the corresponding covariance matrix is shown in equation (5). One group is called the fixed group, denoted as $\hat{\boldsymbol{a}}_1$, which can be reliably fixed, namely with sufficiently high success rate, and the other group is called the unfixed group, denoted as $\hat{\boldsymbol{a}}_2$, whose float estimates need to be corrected according to the fixed ambiguity group:

$$\hat{\boldsymbol{a}} = \begin{bmatrix} \hat{\boldsymbol{a}}_1 \\ \hat{\boldsymbol{a}}_2 \end{bmatrix} \tag{4}$$

$$\boldsymbol{Q}_{\hat{a}\hat{a}} = \begin{bmatrix} \boldsymbol{Q}_{\hat{a}_1\hat{a}_1} & \boldsymbol{Q}_{\hat{a}_1\hat{a}_2} \\ \boldsymbol{Q}_{\hat{a}_2\hat{a}_1} & \boldsymbol{Q}_{\hat{a}_2\hat{a}_2} \end{bmatrix}. \tag{5}$$

The float ambiguity $\hat{\boldsymbol{a}}_2$ is corrected by equation (6) and the corresponding covariance is shown in equation (7):

$$\tilde{\boldsymbol{a}}_2 = \hat{\boldsymbol{a}}_2 - \boldsymbol{Q}_{\hat{a}_2\hat{a}_1} \boldsymbol{Q}_{\hat{a}_1\hat{a}_1}^{-1} (\hat{\boldsymbol{a}}_1 - \tilde{\boldsymbol{a}}_1) \tag{6}$$

$$\boldsymbol{Q}_{\tilde{a}_2\tilde{a}_2} = \boldsymbol{Q}_{\hat{a}_2\hat{a}_2} - \boldsymbol{Q}_{\hat{a}_2\hat{a}_1} \boldsymbol{Q}_{\hat{a}_1\hat{a}_1}^{-1} \boldsymbol{Q}_{\hat{a}_1\hat{a}_2} \tag{7}$$

where $\tilde{\boldsymbol{a}}_1$ is a fixed integer solution corresponding to $\hat{\boldsymbol{a}}_1$, $\tilde{\boldsymbol{a}}_2$ is the corrected float ambiguity and $\boldsymbol{Q}_{\tilde{a}_2\tilde{a}_2}$ is the corresponding covariance matrix.

After the above process, equation (3) can be expressed in the form of the following inverse transform:

$$\tilde{\boldsymbol{n}} = \boldsymbol{Z}^{-T} \tilde{\boldsymbol{a}} = F\tilde{\boldsymbol{a}} = \begin{bmatrix} \boldsymbol{F}_1 & \boldsymbol{F}_2 \end{bmatrix} \begin{bmatrix} \tilde{\boldsymbol{a}}_1 \\ \tilde{\boldsymbol{a}}_2 \end{bmatrix} = \boldsymbol{F}_1 \tilde{\boldsymbol{a}}_1 + \boldsymbol{F}_2 \tilde{\boldsymbol{a}}_2. \tag{8}$$

Obviously, matrix $F = \boldsymbol{Z}^{-T}$, and $\boldsymbol{F}$ is split into two parts, namely $\boldsymbol{F}_1$ corresponding to $\tilde{\boldsymbol{a}}_1$ and $\boldsymbol{F}_2$ corresponding to $\tilde{\boldsymbol{a}}_2$. Note that in the above, $\tilde{\boldsymbol{a}}_1$ will be treated as a known constant without any uncertainty and $\tilde{\boldsymbol{a}}_2$ will be treated as an unknown but with prior information as shown in equations (6) and (7).

2.2. GNSS attitude determination model

As the baseline length in GNSS attitude determination is generally far less than the distance between the antennas and the satellites, the lines of sight for all antennas tracking the same satellite are regarded as the same. At the same time, considering the short-baseline nature, it can be safely assumed that almost all common errors have been completely eliminated in the DD observations, so the DD measurement equations can be simplified as follows:

$$\nabla \Delta \boldsymbol{p}_{0r}^{ij} = -\left(\boldsymbol{L}_r^i - \boldsymbol{L}_r^j \right) \boldsymbol{b}_{0r}^e \tag{9}$$

$$\nabla\Delta\phi_{0r}^{ij} = -\left(\boldsymbol{L}_r^i - \boldsymbol{L}_r^j\right)\boldsymbol{b}_{0r}^e - \lambda\boldsymbol{n}_{0r}^{ij} \tag{10}$$

where $\nabla\Delta$ denotes the DD operator, superscripts i and j denote the ith and jth tracked satellite, and subscripts 0 and r denote the main antenna and slave antenna. Corrected measurements $\nabla\Delta\boldsymbol{p}_{0r}^{ij}$ and $\nabla\Delta\phi_{0r}^{ij}$ denote the observed minus computed double-difference pseudo-range and carrier phase (expressed in unit of meters) measurement vectors, respectively. Vector $\boldsymbol{L}$ denotes the line-of-sight vector, $\boldsymbol{b}_{0r}^e$ denotes the baseline vector expressed in the WGS-84 frame, scalar λ denotes the wavelength, and $\boldsymbol{n}$ denotes the DD float ambiguities.

At the immediately previous epoch, applying the $\boldsymbol{Z}$ transform to float ambiguities $\boldsymbol{n}$ then selecting the partial fixed ambiguities, equation (8) is obtained. In addition, the float estimates in the unfixed ambiguity group, along with the corresponding covariance matrix, are retained and used to assist in IAR at the current epoch if the corresponding satellite is still tracked without cycle slips or with cycle slips correctly repaired. For clarity, the corresponding (pseudo-) measurement equation is displaced in the following:

$$\tilde{\boldsymbol{a}}_2 = \boldsymbol{a}_2 + \boldsymbol{e} \tag{11}$$

in which the covariance matrix of the zero-mean measurement error $\boldsymbol{e}$ is exactly the one shown in equation (7). We stack all measurements shown in equations (9) and (10) to get a measurement vector denoted as $\boldsymbol{p}/\phi$. And the matrix composed of the line-of-sight vector, namely the coefficient matrix of the baseline vector, is $\boldsymbol{A}$. So finally we have the following measurement equation at the current epoch, with equation (8) being taken into consideration:

$$\boldsymbol{d} = \begin{bmatrix} \boldsymbol{p} \\ \psi \\ \tilde{\boldsymbol{a}}_2 \end{bmatrix} = \begin{bmatrix} \boldsymbol{A} & 0 \\ \boldsymbol{A} & \boldsymbol{\Lambda F}_2 \\ 0 & \boldsymbol{I} \end{bmatrix} \begin{bmatrix} \boldsymbol{b} \\ \boldsymbol{a}_2 \end{bmatrix} + \varepsilon = \boldsymbol{C} \begin{bmatrix} \boldsymbol{b} \\ \boldsymbol{a}_2 \end{bmatrix} + \varepsilon \tag{12}$$

where

$$\psi = \phi - \boldsymbol{F}_1\tilde{\boldsymbol{a}}_1 = \boldsymbol{Ab} - \boldsymbol{\Lambda F}_2\boldsymbol{a}_2. \tag{13}$$

Note that the diagonal matrix $\boldsymbol{\Lambda}$ consists of the wavelength λ. For convenience, the coefficient matrix of parameters $\boldsymbol{b}$ and $\boldsymbol{a}_2$ denotes $\boldsymbol{C} = \begin{bmatrix} \boldsymbol{A} & 0 \\ \boldsymbol{A} & \boldsymbol{\Lambda F}_2 \\ 0 & \boldsymbol{I} \end{bmatrix}$ with identity matrix $\boldsymbol{I}$.

A point worth emphasizing is that equation (12) is exactly the measurement model for the estimation or adjustment at the current epoch. The BC approach, detailed in the following section 2.3, can be performed when the parameters $\boldsymbol{b}$ and $\boldsymbol{a}_2$ in equation (12) have been estimated. By modifying equation (12), namely replacing $\boldsymbol{b}$ with (increment) AAs as parameters, the AA approach, detailed in the following section 2.4, would be executed. For either of the two approaches, PAR processing would be performed to fix potential parts of estimate $\boldsymbol{a}_2$, detailed in the above section 2.1.

2.3. BC approach

The BC approach is simply solving the problem with exactly the same measurement equation as in equation (12). The weight matrix is denoted as $\boldsymbol{K} = (\mathrm{cov}[\varepsilon])^{-1}$, and we can easily derive the following least-squares solution:

$$\boldsymbol{P} = \left(\boldsymbol{C}^T\boldsymbol{KC}\right)^{-1} = \begin{bmatrix} \boldsymbol{P}_{\widehat{b}\,\widehat{b}} & \boldsymbol{P}_{\widehat{b}\,\widehat{a}_2} \\ \boldsymbol{P}_{\widehat{a}_2\,\widehat{b}} & \boldsymbol{P}_{\widehat{a}_2\,\widehat{a}_2} \end{bmatrix} \tag{14}$$

$$\begin{bmatrix} \widehat{\boldsymbol{b}} \\ \widehat{\boldsymbol{a}}_2 \end{bmatrix} = \boldsymbol{PC}^T\boldsymbol{Kd}. \tag{15}$$

We extract float ambiguities $\widehat{\boldsymbol{a}}_2$ and the corresponding covariance matrix $\boldsymbol{P}_{\widehat{a}_2\,\widehat{a}_2}$ from equations (15) and (14) for decorrelation processing. According to the PAR theory, the float ambiguity $\widehat{\boldsymbol{a}}_2$ after decorrelation is denoted as $\hat{\boldsymbol{u}}$, and if a part of $\hat{\boldsymbol{u}}$ can be fixed, we introduce the following splitting:

$$\hat{\boldsymbol{u}} = \begin{bmatrix} \hat{\boldsymbol{u}}_1 & \hat{\boldsymbol{u}}_2 \end{bmatrix}^T. \tag{16}$$

Following equations (6)–(8), we readily have the following. Note that the meanings of matrices $\boldsymbol{J}$, $\boldsymbol{J}_1$ and $\boldsymbol{J}_2$ are similar to those of the matrices $\boldsymbol{F}$, $\boldsymbol{F}_1$ and $\boldsymbol{F}_2$ in equation (8), respectively:

$$\breve{\boldsymbol{a}}_2 = \boldsymbol{J}\tilde{\boldsymbol{u}} = \boldsymbol{J}_1\tilde{\boldsymbol{u}}_1 + \boldsymbol{J}_2\tilde{\boldsymbol{u}}_2. \tag{17}$$

Substituting equation (17) into equation (8), we have the following.

$$\tilde{\boldsymbol{n}} = \boldsymbol{F}_1\tilde{\boldsymbol{a}}_1 + \boldsymbol{F}_2\boldsymbol{J}_1\tilde{\boldsymbol{u}}_1 + \boldsymbol{F}_2\boldsymbol{J}_2\tilde{\boldsymbol{u}}_2. \tag{18}$$

We replace $\boldsymbol{F}_1\tilde{\boldsymbol{a}}_1$ with $\boldsymbol{F}_1\tilde{\boldsymbol{a}}_1 + \boldsymbol{F}_2\boldsymbol{J}_1\tilde{\boldsymbol{u}}_1$, replace $\boldsymbol{F}_2$ with $\boldsymbol{F}_2\boldsymbol{J}_2$, and replace $\tilde{\boldsymbol{a}}_2$ with $\tilde{\boldsymbol{u}}_2$, and the processing can go on to the next epoch.

After the optimal value of float ambiguity $\breve{\boldsymbol{a}}_2$ in equation (17) is obtained, and hence $\boldsymbol{P}_{\widehat{b}\,\widehat{a}_2}$ and $\boldsymbol{P}_{\widehat{a}_2\,\widehat{a}_2}$ are extracted from equation (14), then the baseline vector $\widehat{\boldsymbol{b}}$ will be corrected according to equation (19); namely the optimal value of the baseline vector $\breve{\boldsymbol{b}}$ in the WGS-84 coordinate system is obtained:

$$\breve{\boldsymbol{b}} = \widehat{\boldsymbol{b}} - \boldsymbol{P}_{\widehat{b}\,\widehat{a}_2}\boldsymbol{P}_{\widehat{a}_2\,\widehat{a}_2}^{-1}\left(\widehat{\boldsymbol{a}}_2 - \breve{\boldsymbol{a}}_2\right). \tag{19}$$

For attitude determination, the baseline coordinate vector in the BF is usually known, denoted as $\boldsymbol{b}_{0r}^c = [x^c, y^c, z^c]^T$. The baseline vector calculated in equation (19) is firstly transformed to the one in the LLS, denoted as $\boldsymbol{b}_{0r}^l = \left[x^l, y^l, z^l\right]^T = \boldsymbol{R}_e^l\breve{\boldsymbol{b}}$. So we have the following rotation transformation:

$$\boldsymbol{b}_{0r}^l = \boldsymbol{R}^T(\varphi, \omega, \gamma)\boldsymbol{b}_{0r}^c \tag{20}$$

with the rotation matrix represented by the attitude as follows:

$$\boldsymbol{R}(\varphi,\omega,\gamma)=\begin{bmatrix}\cos\gamma\cos\varphi-\sin\gamma\sin\omega\sin\varphi & \cos\gamma\sin\varphi+\sin\gamma\sin\omega\cos\varphi & -\sin\gamma\cos\omega\\ -\cos\omega\sin\gamma & \cos\omega\cos\varphi & \sin\omega\\ \sin\gamma\cos\varphi+\cos\gamma\sin\omega\sin\varphi & \sin\gamma\sin\varphi-\cos\gamma\sin\omega\cos\varphi & \cos\gamma\cos\omega\end{bmatrix}. \tag{21}$$

Without loss of generality, let $\boldsymbol{b}_{12}^{c}=\begin{bmatrix}0 & l_2 & 0\end{bmatrix}^T$ and $\boldsymbol{b}_{13}^{c}=\begin{bmatrix}l_3\sin\beta & l_3\cos\beta & 0\end{bmatrix}^T$ with known β, as shown in figure 1. Let $\boldsymbol{b}_{12}^{l}=\begin{bmatrix}x_2 & y_2 & z_2\end{bmatrix}^T$ and $\boldsymbol{b}_{13}^{l}=\begin{bmatrix}x_3 & y_3 & z_3\end{bmatrix}^T$. According to equations (20) and (21), the AAs are calculated as follows:

$$\begin{aligned}\varphi&=-\arctan(x_2/y_2)\\ \omega&=\arctan\left(z_2/\sqrt{(x_2)^2+(y_2)^2}\right)\\ \gamma&=\arcsin\left(\frac{\sin\omega\cos\beta l_3-z_3}{\cos\omega\sin\beta l_3}\right).\end{aligned} \tag{22}$$

When the number of fixed double-difference ambiguities is less than three, the BC approach, described above, is selected to determine the AAs. In the BC approach, the baseline coordinate vectors are obtained in a linear equation; however, in order to calculate three AAs, the two baselines need to be resolved, namely six baseline parameters are calculated to solve the three-parameter attitude problem. Obviously, the parameter redundancy is introduced, which decreases the model strength and increases the solution variance.

2.4. AA approach

From the above, we readily have the relationship: $\boldsymbol{b}=\boldsymbol{R}_l^e\boldsymbol{b}_{0r}^l=\boldsymbol{R}_l^e\boldsymbol{R}^T(\varphi,\omega,\gamma)\boldsymbol{b}_{0r}^c$, on the right hand side of which there are only three unknowns, namely φ, ω and γ. Substituting this relationship into equation (12), we get the measurement equation for the AA approach. Clearly from equation (21), this measurement equation is nonlinear, hence linearizing equation (21) as follows:

$$\begin{aligned}\boldsymbol{R}^T(\varphi,\omega,\gamma)=\boldsymbol{R}^T(\varphi_0,\omega_0,\gamma_0)+\frac{\partial\boldsymbol{R}^T(\varphi_0,\omega_0,\gamma_0)}{\partial\varphi}\delta\varphi\\ +\frac{\partial\boldsymbol{R}^T(\varphi_0,\omega_0,\gamma_0)}{\partial\omega}\delta\omega+\frac{\partial\boldsymbol{R}^T(\varphi_0,\omega_0,\gamma_0)}{\partial\gamma}\delta\gamma\end{aligned} \tag{23}$$

with

$$\begin{aligned}\frac{\partial\boldsymbol{R}^T}{\partial\omega}&=\begin{bmatrix}-S\varphi_0C\omega_0S\gamma_0 & S\varphi_0S\omega_0 & S\varphi_0C\omega_0C\gamma_0\\ C\varphi_0C\omega_0S\gamma_0 & -C\varphi_0S\omega_0 & -C\varphi_0C\omega_0C\gamma_0\\ S\varphi_0S\gamma_0 & C\omega_0 & -S\omega_0C\gamma_0\end{bmatrix}\\ \frac{\partial\boldsymbol{R}^T}{\partial\gamma}&=\begin{bmatrix}-C\varphi_0S\gamma_0-S\varphi_0S\omega_0C\gamma_0 & 0 & C\varphi_0C\gamma_0-S\varphi_0S\omega_0S\gamma_0\\ -S\varphi_0S\gamma_0+C\varphi_0S\omega_0C\gamma_0 & 0 & S\varphi_0C\gamma_0+C\varphi_0S\omega_0S\gamma_0\\ -C\omega_0C\gamma_0 & 0 & -C\omega_0S\gamma_0\end{bmatrix}\\ \frac{\partial\boldsymbol{R}^T}{\partial\varphi}&=\begin{bmatrix}-C\gamma_0S\varphi_0-C\varphi_0S\omega_0S\gamma_0 & -C\varphi_0C\omega_0 & -S\gamma_0S\varphi_0+C\varphi_0S\omega_0C\gamma_0\\ C\varphi_0C\gamma_0-S\varphi_0S\omega_0S\gamma_0 & -S\varphi_0C\omega_0 & C\varphi_0S\gamma_0+S\varphi_0S\omega_0C\gamma_0\\ 0 & 0 & 0\end{bmatrix}\end{aligned} \tag{24}$$

where S denotes *sin*, C denotes *cos*, and φ_0, ω_0, γ_0 denote the initial values of yaw, pitch and roll angles, respectively, which can be calculated from the BC approach, as shown in the above section 2.3. In equation (23), $\delta\varphi$, $\delta\omega$ and $\delta\gamma$ denote the AA corrections, or increment AAs. With equation (23) being taken into consideration, we replace $\boldsymbol{b}$ in equation (12) with (increment) AAs $\boldsymbol{\theta}$ as parameters. Meanwhile, the coefficient matrix of parameters $\boldsymbol{\theta}$ and $\boldsymbol{u}_2$ denotes $\boldsymbol{M}$, and hence the following linearized equation is obtained:

$$\boldsymbol{c}=\begin{bmatrix}\boldsymbol{p}\\ \boldsymbol{\psi}\\ \tilde{\boldsymbol{u}}_2\end{bmatrix}=\boldsymbol{M}\begin{bmatrix}\boldsymbol{\theta}\\ \boldsymbol{u_2}\end{bmatrix}+\zeta \tag{25}$$

where

$$\boldsymbol{\theta}=\begin{bmatrix}\delta\varphi & \delta\omega & \delta\gamma\end{bmatrix}^T. \tag{26}$$

Note that equation (25) is exactly the linearized measurement equation for the AA approach. The least-squares solution of equation (25) is shown as follows, with cofactor matrix

$$\begin{aligned}\boldsymbol{G}&=\begin{bmatrix}\boldsymbol{T} & 0\\ 0 & \bar{\boldsymbol{P}}\end{bmatrix}.\\ \boldsymbol{N}&=\left(\boldsymbol{M}^T\boldsymbol{G}^{-1}\boldsymbol{M}\right)^{-1}=\begin{bmatrix}\boldsymbol{N}_{\hat{\theta}\hat{\theta}} & \boldsymbol{N}_{\hat{\theta}\hat{u}_2}\\ \boldsymbol{N}_{\hat{u}_2\hat{\theta}} & \boldsymbol{N}_{\hat{u}_2\hat{u}_2}\end{bmatrix}\end{aligned} \tag{27}$$

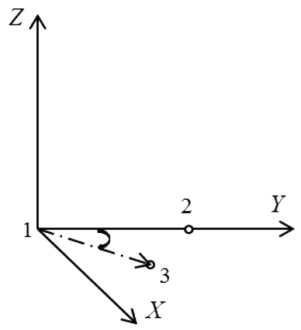

Figure 1. Antenna configuration in the BF.

$$\begin{bmatrix} \hat{\boldsymbol{\theta}} \\ \hat{\boldsymbol{u}}_2 \end{bmatrix} = \boldsymbol{N}\boldsymbol{M}^T\boldsymbol{G}^{-1}\boldsymbol{c} \tag{28}$$

where $\boldsymbol{T}$ is the cofactor matrix corresponding to the measurements $\boldsymbol{p}$ and ψ, and $\bar{\boldsymbol{P}}$ is equivalent to $\boldsymbol{Q}_{\breve{u}_2\breve{u}_2}$. Since the observation equation is nonlinear, the iterative method is used to obtain the optimal AAs. In this contribution, when the Euclidean norm of the AA corrections is less than 10^{-7}, we will stop the iteration, and output the optimal attitude values and float ambiguities. Then we extract $\hat{\boldsymbol{u}}_2$ and $\boldsymbol{N}_{\hat{u}_2\hat{u}_2}$ from equations (28) and (27), and the PAR is completely parallel to that in the above section 2.3.

Compared with the BC approach, the three-parameter AAs are directly calculated in the AA approach, but the equation is nonlinear. Clearly, it will produce linearization errors whose magnitude directly depends on the accuracy of the initial attitude estimates. Obviously, the two parameterizations have their merits and demerits. To avoid the demerits of the two parameterizations and combine their merits, a switching strategy is proposed. Namely, as long as there are at least three un-ambiguous carrier phase measurements, we deem that the initial attitude estimate is sufficiently accurate, the linearization errors can be regarded as sufficiently small to be neglected, and the AA approach is employed; otherwise, the BC approach is adopted. Note that the AA approach needs the initial attitude estimate calculated by the BC approach to linearize the observation model, namely the BC approach is also used as a preprocessing step of AA approach.

3. Experiment

In order to verify the performance of the proposed method, we carried out static and kinematic experiments. In the static experiment, the proposed method is compared with the BC and AA methods. The stability and accuracy of the calculated attitude, and the fixed speed of ambiguity are shown. In the kinematic experiment, we calculated the yaw angle of the vehicle and showed the vehicle's driving route in real time.

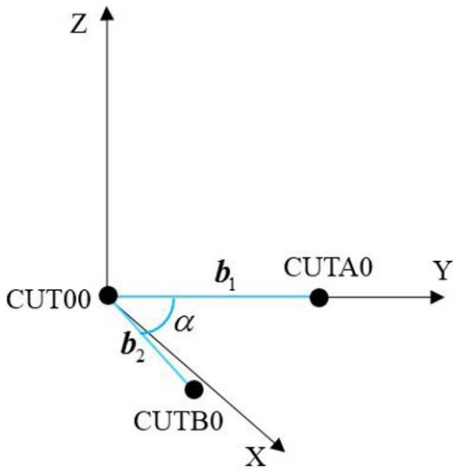

Figure 2. The antennas' location in the BF in the static experiment.

Table 1. The antenna coordinates in WGS-84 frame.

Antennas	X(m)	Y(m)	Z(m)
CUT00	−2364 337.44	4870 285.62	−3360 809.67
CUTA0	−2364 335.42	4870 281.46	−3360 816.71
CUTB0	−2364 333.54	4870 287.34	−3360 809.53

3.1. Static experiment

The experimental data are downloaded from the GNSS Research Center at Curtin University. The data are collected from the CUTB0, CUT00 and CUTA0 antennas of the TRIMBLE NETR9 receiver with the frequency of 1 Hz and 10° elevation mask angle. All antennas are located on the roof of the building, which assists to reduce the impact of multipath effects on observation data. The antennas' actual distribution and location in the BF are shown in [28] and figure 2, respectively. The antenna CUT00 is selected as the main antenna, while antenna CUTA0 and antenna CUTB0 are selected as the slave antennas. The known coordinates of each antenna in the WGS-84 coordinate system are shown in table 1, and after a certain transformation, the calculated baseline coordinate vector $\boldsymbol{b}_1$ is (0, 8.42, 0) and $\boldsymbol{b}_2$ is (4.269, −0.035, 0) in the BF. The lengths of these two baseline vectors are 8.42 m and 4.27 m, respectively. In addition, the calculated reference yaw, pitch and roll angles are 179.9938°, –1.3217° and 2.8711°, respectively.

In order to verify the performance of the proposed switching-parameterization (SP) approach, this approach is compared with the BC and AA approaches. In the data processing, the fixing success rate threshold $\boldsymbol{P}_0$ and the ratio value are set to 98% and 2, respectively. Figure 3(a) shows the number of visible satellites in the static experiment. It can be seen that the visible satellite number is stable and changes from 8 to 7 in around 1800 epochs. The number of fixed ambiguities of three methods is shown in figure 3(b). For clarity, the different marker sizes are used in the drawing of partial enlargement. It is obvious that all ambiguities are fixed within five epochs for the SP approach. In addition, the fixed speed of the proposed approach is faster than the other two approachs. Specifically,

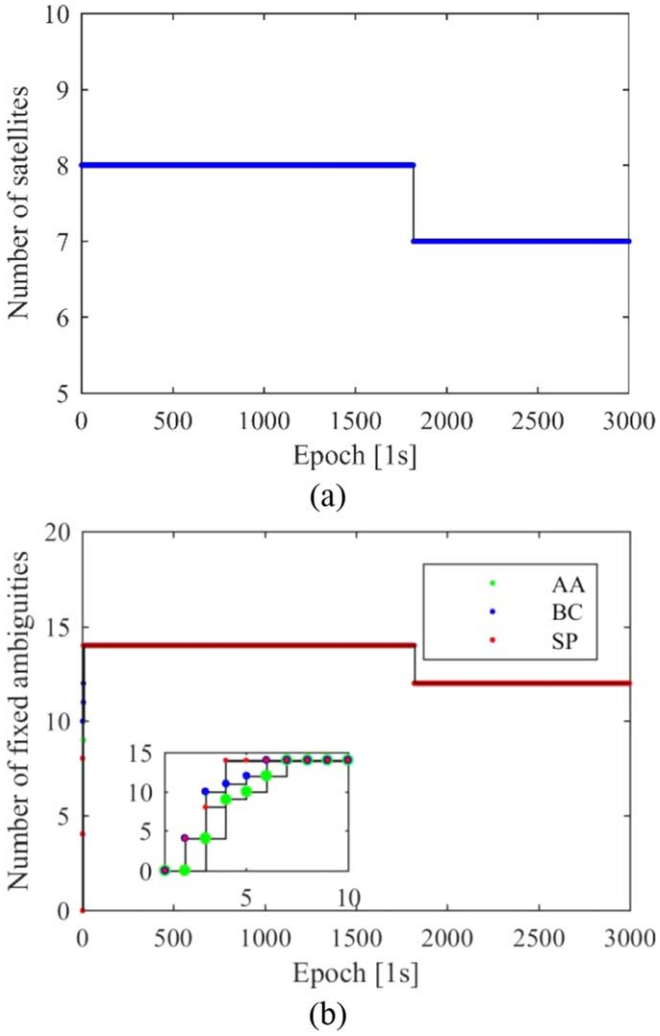

Figure 3. The visible satellite number (a) and the fixed ambiguity number (b) in the static experiment.

Table 2. The bootstrapped success rates of the proposed approach for both baseline vectors.

	Epoch				
	1	2	3	4	
$\boldsymbol{b}_1$	43.16%	95.61%	90.49%	97.85%	100%
$\boldsymbol{b}_2$	74.74%	92.10%	99.98%	100%	100%

for the proposed approach, the bootstrapped success rates of the unfixed ambiguities corresponding to two baseline vectors are shown in table 2. At the initial epoch, the overall bootstrapped success rate of baseline 2 is higher than baseline 1, which is due to the different geometries, namely directions, of the two baselines. The reason why the number of success rates is two at the fourth epoch is that the AA approach is used for attitude determination at this epoch, hence the float ambiguities are fixed twice, namely using the estimates in the BC and AA solutions, respectively.

Table 3 shows the averaged attitude values of the proposed approach within 10 epochs. We can see that the average values of the three AAs in the first 10 epochs are far from their

Table 3. The averaged attitude values of the proposed approach within 10 epochs.

	1–10 epochs	11–20 epochs	21–30 epochs	31–40 epochs
Yaw (°)	180.3155	180.0058	180.0056	179.9986
Pitch (°)	−0.8242	−1.2479	−1.2457	−1.2717
Roll (°)	3.2831	2.9083	2.9268	2.9653

Table 4. AA statistics of three approaches in the static experiment.

Type	SP		BC		AA	
	RMS	STD	RMS	STD	RMS	STD
Yaw (°)	0.0152	0.0123	0.0143	0.0134	0.0152	0.0123
Pitch (°)	0.0382	0.0375	0.0531	0.0469	0.0382	0.0375
Roll (°)	0.0669	0.0630	0.0782	0.0744	0.0668	0.0630

corresponding reference values. That is because the number of fixed ambiguities is low. The determined AAs become closer and closer to the reference values as the epoch increases. Once all ambiguities are fixed, the attitude determination accuracy stays rather stationary, due to the fact that this is a static experiment, in which the geometry of the baseline constellation only varies slowly.

Figures 4(a) and (b) show the AA errors of the SP and BC approaches when the whole ambiguities are fixed. Note that the SP and AA approaches are equivalent to each other when the whole ambiguities are fixed, and hence the attitude errors of the AA approach are not shown. The statistics of the SP, BC and AA approaches are listed in table 4. It can be seen from figure 4(a) that the AA errors, namely the AAs determined by the proposed method minus the corresponding reference values, are concentrated around 0°. In addition, the range of the yaw angle fluctuation is the smallest, the pitch angle is the second one, and the roll angle fluctuation is the largest. Obviously, the same goes for the AA errors calculated by the BC approach. This fluctuation information can also be derived from standard deviation (STD) listed in table 4. Compared with the BC approach, the STD values of the SP approach are smaller in yaw, pitch and roll angles. And hence we know that the attitude calculated by the proposed approach is relatively stable. Meanwhile, table 4 gives the root mean square (RMS) of the three-parameter AAs. From table 4, it is not difficult to find that the proposed approach has a higher precision than the BC approach, especially in the pitch and roll angles. Specifically, the RMS of the yaw is approximately 0.01°, the RMS of the pitch angle is within 0.04°, and the RMS of the roll angle is as high as 0.07°.

3.2. *Kinematic experiment*

Limited to the existing test condition, two GNSS receivers are used to collect the experimental data whose sampling interval is set to 1 s and the cutoff satellite elevation angle is set to 10°. The distance between the two antennas connected rigidly to the vehicle is 0.65 m and the connection direction is perpendicular to the driving direction of the vehicle. The actual position of the two antennas on the vehicle and their location in

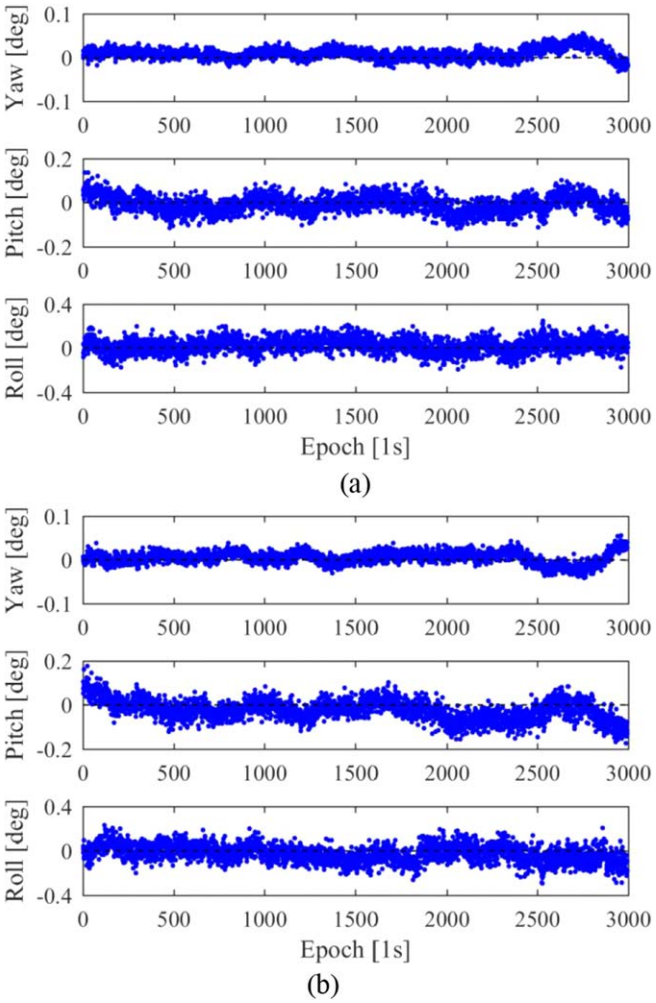

Figure 4. The calculated AA errors of the SP (a) and BC (b) approaches.

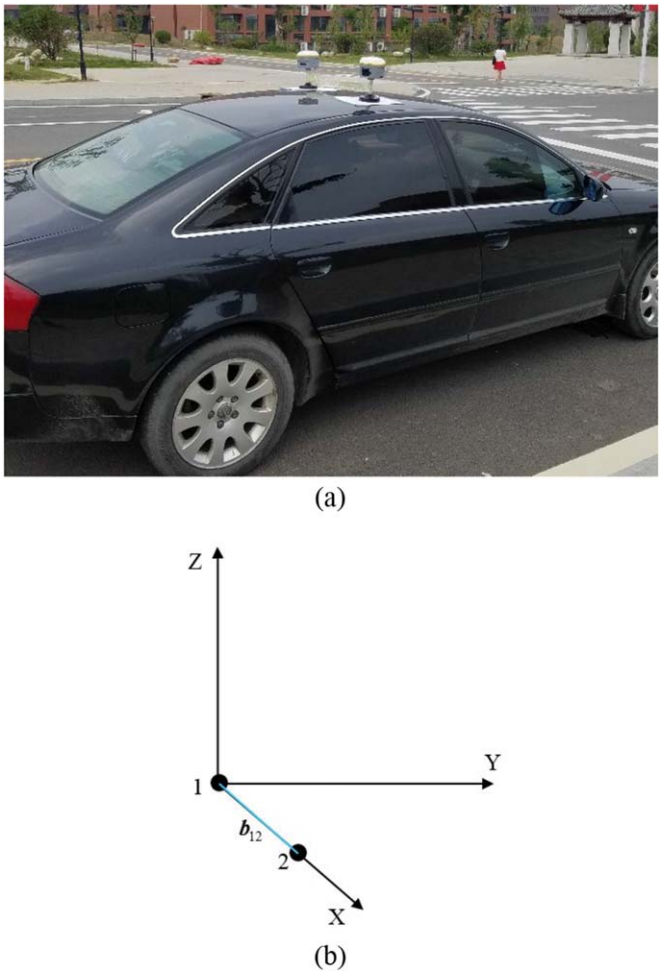

Figure 5. The antenna configuration in the kinematic experiment: (a) the actual antenna distribution; (b) the antennas' location in the BF.

the BF are shown in figures 5(a) and (b). The vehicle remains stationary for about five minutes before maneuvering.

Only two antennas are used in the kinematic experiment, and hence the AAs can only be determined by the BC approach, since with the baseline length constraints considered, the BC and AA approaches are equivalent to each other. The settings for the fixing success rate threshold and the ratio value are same as that of the static experiment. During the whole process of vehicle driving, affected by traffic flow, tree occlusion, etc, a large amount of invalid data appeared. Only a part of the data was selected for processing. The first part of the selected data was collected when the vehicle was stationary, and the latter part was collected during the movement.

Figure 6 shows the number of visible satellites. From figure 6, it can be observed that the number of visible satellites was 10 before about 400 epochs. It changes frequently and concentrates around 9 or 10 due to maneuvering and other factors. The actual driving route and the corresponding yaw angle are shown in figure 7. By comparing these two figures, it can be observed that the yaw angle generally matches the actual driving route, and the changes in yaw angle are clear at the turn of the route.

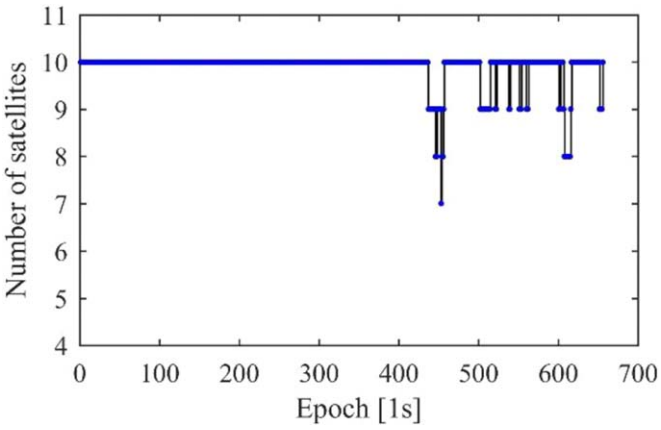

Figure 6. The visible satellite number in the kinematic experiment.

The baseline length error and the roll angle are calculated and shown in figures 8 and 9, respectively. It can be observed that the error of the baseline length is around zero, which shows a satisfactory accuracy of the solution. The baseline

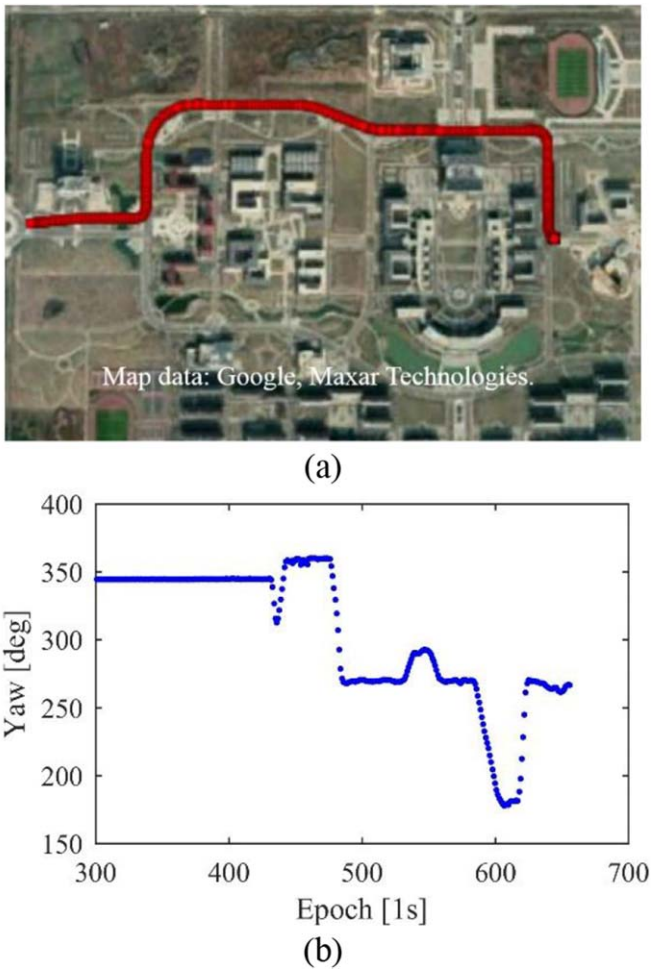

Figure 7. The comparison figures in the kinematic experiment: (a) the actual driving route (map data: Google, Maxar Technologies) and (b) the corresponding yaw angle. (Map data: Google, Maxar Technologies.)

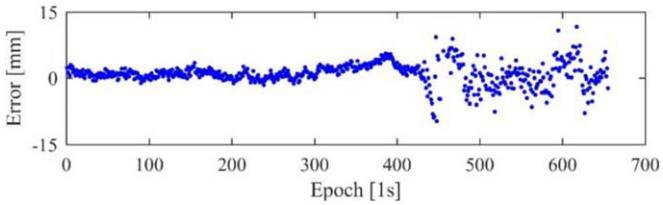

Figure 8. The error of the baseline length in the kinematic experiment.

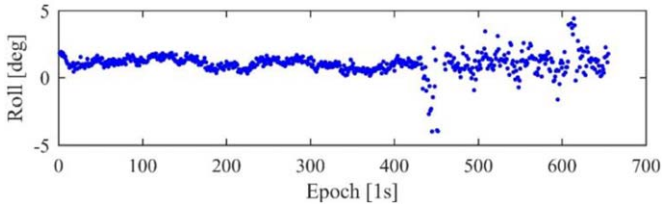

Figure 9. The roll angle in the kinematic experiment.

length error and roll angle for the latter part of the data have greater fluctuations than the previous part, implying that the solution result in the kinematic environment is not as good as that in the static environment. One of the obvious fluctuations is concentrated around 450 epochs, at which the vehicle is moving. It can be easily found that these fluctuations correspond to the change of the visible satellite number, namely the number of visible satellites dropped from 10 to 9 or even 7 around these epochs.

4. Conclusions

Correctly fixing the integer ambiguities and selecting the appropriate attitude determination method are crucial for determining the attitude using the GNSS measurements. In this contribution, PAR is used to fix the integer ambiguities. The partial ambiguities with bootstrapped success rate above a given threshold are reliably fixed. The estimates of the unfixed ambiguities, along with the corresponding covariance matrix, are retained to the next epoch as a set of pseudo-measurements to assist the estimation at that epoch. A switching strategy is used for attitude determination; namely, at any epoch, BC is resolved first, and AA parameterization is further employed if there are at least three un-ambiguous carrier phase measurements.

The performance of the proposed method is verified by static and kinematic experiments. In addition, a comparative study is implemented with the BC and AA methods in the static experiment. The static experimental results show that all ambiguities can be fixed within five epochs for the proposed method, and it is faster than the other two methods. In addition, the higher-precision AAs can be obtained by the SP method. Concretely, the accuracy of the yaw angle, pitch angle and roll angle is approximately 0.01°, 0.03° and 0.06° in terms of RMS, respectively. Meanwhile, in contrast to the BC approach, the AAs are relatively stable. The kinematic experimental results indicate that the yaw angle is consistent with the actual driving route of the vehicle, but the error of baseline length and the calculated roll angle fluctuate greatly due to the fluctuation in the number of visible satellites.

Acknowledgments

This work was funded by the National Natural Science Foundation of China (Grant Nos. 41774005 and 41774026) and the China Postdoctoral Science Foundation (Grant Nos. 2019M652010 and 2019T120477).

ORCID iD

Guobin Chang https://orcid.org/0000-0001-6392-3265

References

[1] Giorgi G, Teunissen P J G, Verhagen S and Buist P J 2010 Testing a new multivariate GNSS carrier phase attitude determination method for remote sensing platforms *Adv. Space Res.* **46** 118–29

[2] Li Y, Zhang K, Roberts C and Murata M 2004 On-the-fly GPS-based attitude determination using single- and double-differenced carrier phase measurements *GPS Solut.* **8** 93–102

[3] Giorgi G, Teunissen P J G and Gourlay T P 2012 Instantaneous Global Navigation Satellite System (GNSS)-based attitude determination for maritime applications *IEEE J. Oceanic Eng.* **37** 348–62

[4] He J, Huang X and Wang G 2008 Design and application of single-antenna GPS/accelerometers attitude determination system *J. Syst. Eng. Electron*. **19** 220–7

[5] Li W, Liu M and Duan D 2014 Adaptive Huber-based Kalman filtering for spacecraft attitude estimation *Trans. Inst. Meas. Control*. **36** 828–36

[6] Zhang X, Wu M and Liu W 2015 Receiver time misalignment correction for GPS-based attitude determination *J. Navig.* **68** 646–64

[7] Xu P, Shu Y, Niu X, Liu J, Yao W and Chen Q 2019 High-rate multi-GNSS attitude determination: experiments, comparisons with inertial measurement units and applications of GNSS rotational seismology to the 2011 Tohoku Mw9. 0 earthquake *Meas. Sci. Technol.* **30** 024003

[8] Fu S, Li Y, Zhang M, Zong K, Cheng L and Wu M 2017 Ultra-wideband pose detection system for boom-type roadheader based on Caffery transform and Taylor series expansion *Meas. Sci. Technol.* **29** 015101

[9] Chang G, Xu T and Wang Q 2016 Baseline configuration for GNSS attitude determination with an analytical least-squares solution *Meas. Sci. Technol.* **27** 125105

[10] Xia K, Zhang X, Gao J and Zhang L 2008 Study on GPS attitude determination technology based on QPSO algorithm *Proc. 7th WCICA* (*Chongqing, China*)

[11] Kim D and Langley R B 1999 An optimized least-squares technique for improving ambiguity resolution and computational efficiency *Proc. 12th ION-ITM* (*Nashville, TN*)

[12] Frei E 1990 Rapid static positioning based on the fast ambiguity resolution approach FARA: theory and first results *Manuscr. Geod.* **15** 325–56

[13] Teunissen P J G 1995 The least-squares ambiguity decorrelation adjustment: a method for fast GPS integer ambiguity estimation *J. Geod.* **70** 65–82

[14] Teunissen P J G, Giorgi G and Buist P J 2010 Testing of a new single-frequency GNSS carrier phase attitude determination method: land, ship and aircraft experiments *GPS Solut.* **15** 15–28

[15] Chen W and Sun X 2016 Performance improvement of GPS single frequency, single epoch attitude determination with poor satellite visibility *Meas. Sci. Technol.* **27** 075104

[16] Wang B, Deng Z, Wang S and Fu M 2010 A motion-based integer ambiguity resolution method for attitude determination using the global positioning system (GPS) *Meas. Sci. Technol.* **21** 065102

[17] Teunissen P 2006 The lambda method for the GNSS compass *Artif. Satell.* **41** 89–103

[18] Wu M, He J and Wang H 2016 Reliable single epoch ambiguity resolution for precise attitude determination using BeiDou triple-frequency observations *J. Chin. Inertial Technol.* **24** 624–32

[19] Teunissen P J G, Joosten P and Tiberius C C J M 1999 Geometry-free ambiguity success rates in case of partial fixing *Proc. ION-NTM* (*San Diego, CA*)

[20] Parkins A 2010 Increasing GNSS RTK availability with a new single-epoch batch partial ambiguity resolution algorithm *GPS Solut.* **15** 391–402

[21] Shu B, Liu H, Zhang J, Pan G and Jiang J 2017 Performance assessment of partial ambiguity resolution based on BDS/GPS combined positioning *Geomatics Inf. Sci. Wuhan Univ.* **42** 989–94

[22] Cheng J, Wang J and Zhao L 2014 A direct attitude determination approach based on GPS double-difference carrier phase measurements *J. Appl. Math.* **2014** 1–6

[23] Zhao L, Li N, Li L, Zhang Y and Cheng C 2017 Real-Time GNSS-based attitude determination in the measurement domain *Sensors* **17** 296

[24] Chang G, Xu T, Wang Q, Li S and Deng K 2017 GNSS attitude determination method through vectorization approach *IET Radar Sonar Navig.* **11** 1477–82

[25] Ozgoren M K 2019 Comparative study of attitude control methods based on Euler angles quaternions angle–axis pairs and orientation matrices *Trans. Inst. Meas. Control* **41** 1189–206

[26] Markley F L and Crassidis J L 2014 *Fundamentals of Spacecraft Attitude Determination and Control* (New York: Springer)

[27] Feng Y and Wang J 2010 Computed success rates of various carrier phase integer estimation solutions and their comparison with statistical success rates *J. Geod.* **85** 93–103

[28] GNSS CORS Receiver Setup 2016 (http://saegnss2.curtin.edu.au/ldc/CU-GNSS-receivers-setup.pdf) (Accessed 16 June 2016)